FIELD PATTERNS IN LOSSY CYLINDERS DUE TO A CONCENTRIC HELIX

BY

RICHARD CHARLES HALL

B.S., Purdue University, 1981

THESIS

Submitted in partial fulfillment of the requirements
for the degree of Master of Science in Electrical Engineering
in the Graduate College of the
University of Illinois at Urbana-Champaign, 1983

Urbana, Illinois

ABSTRACT

A theoretical study of the fields inside a homogeneous, lossy cylinder produced by a helix that surrounds the cylinder is presented. The helix is modelled by a single ring of magnetic current surrounding the cylinder. The ring is converted to an equivalent system of cylinders via the Fourier transform so that the boundary-value problem may be solved. Finally, the inverse Fourier transform is taken numerically.

The cylinder is used as a first approximation to the human body so that heating patterns within the body due to electromagnetic wave absorption may be predicted. This study could lead to more effective hyperthermia applicators for regional body heating in the frequency range of 10 to 100 MHz.

Acknowledgment

The author wishes to thank his advisor, Professor Raj Mittra, and Professor Charles Cain for many helpful suggestions, encouragement and support while this work was being performed.

TABLE OF CONTENTS

1. INTRODUCTION

Hyperthermia, the heating of body tissues to above normal temperatures, has been shown to be effective in treating certain cancerous tumors either when used alone or in combination with radiation or drugs [1]. Applicators covering almost the entire frequency range from ultrasound to microwaves are currently being designed and implemented for trial use in the laboratory or clinic. The research covered by this report concerns the design of a radio frequency (10 to 100 MHz) applicator to produce regional heating.

A desirable applicator would focus the energy to produce relatively high temperatures at the core of the body and would be simple to operate and control. A helix surrounding the body, as in Figure 1, operating in the RF range meets nearly all of these requirements. The wavenumber of biological tissue in the RF frequency range allows reasonable penitration [2]; however, because of the long wavelength at these frequencies little focusing of the electromagnetic energy is possible. At higher frequencies, greater focusing can be achieved but biological tissue becomes very lossy at these frequencies reducing penitration. Also the interface between the applicator and the skin becomes critical at high frequencies to reduce the reflection of energy back to the source. At ultrasonic frequencies a pressure wave is used to produce heating. Here, again, the applicator/skin interface is critical and air pockets in the body block the ultrasonic-wave reducing penitration.

The applicator design studied here has the correct E-field orientation for deep heating. The electric field is always parallel to

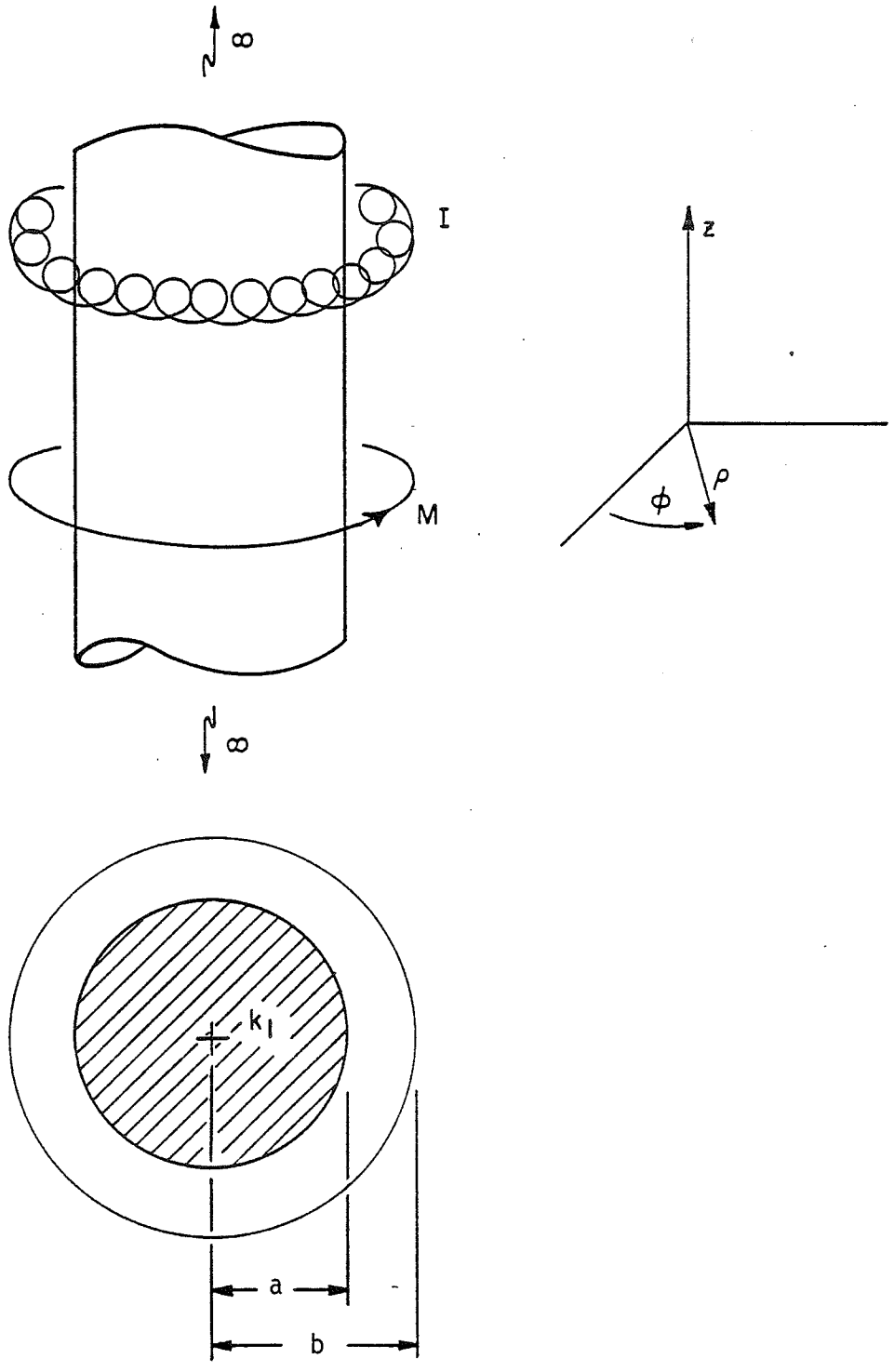

Figure 1. Applicator under study and coordinate system

the muscle/fat interfaces within the body so reflections between tissue layers and between the skin and the applicator are minimized. Thus the applicator/skin interface is less critical than with other types of applicators.

Previous authors have studied the problem of fields inside a cylinder of biological tissue. The cylinder is chosen because of its simple shape and because it is a good model of certain parts of the body to analyze regional heating. Wu and Tsai calculated the fields inside an arbitrarily cross sectioned cylinder due to a plane wave incident by forming an integral equation and using moment method techniques to solve for the fields [3]. Morita and Andersen studied the fields in a homogeneous cylinder produced by electric and magnetic line sources by forming exact solutions using a series of Hankel functions [4].

Here the field patterns of a helix surrounding a homogenous cylinder are studied by forming an exact integral solution for a model of the source and inverting the integral numerically. The model of the source is constructed by noting that the dual to a small electric current loop is a magnetic dipole [5]. Thus, the series of electric current loops that make up the helix can be thought of as a single filament of magnetic current. The integral solution is formed by converting the filamentary ring to an equivalent system of cylinders via the Fourier transform, solving the transformed boundary value problem, and applying the inverse Fourier transform.

A very similar derivation which studied surface waves on dielectric cylinders was done in 1959 by J.W. Duncan [6]. He formulated the integral solution for the fields external to the cylinder and evaluated

it as a contour integral by applying Cauchy's theorem and obtained the far-zone fields by means of a saddle-point integration. A similar integral solution is formulated in this thesis for the fields inside the cylinder and is solved numerically using the Fast Fourier Transform algorithm.

2. MATHEMATICAL FORMULATION

The problem to be investigated is illustrated in Figure 1. An infinitely long dielectric cylinder is oriented so that its axis corresponds to the z axis of a cylindrical coordinate system (ρ,θ,z). The cylinder is lossy with complex wave number k_1, and is surrounded by infinite free space with wave number $k=\sqrt{\mu_0\varepsilon_0}$ The radius of the cylinder is a. Surrounding the cylinder is a filamentary ring of magnetic current of radius b with no z or ϕ variation. Mathematically this is represented using Dirac delta functions as

$$\bar{\kappa}=\hat{\phi}\delta(\rho-b)\delta(z) \quad \text{VOLTS}^2/\text{METER} \tag{2.1}$$

with $\hat{\phi}$ representing a unit vector in the ϕ direction. The source is of unit magnitude such that

$$\int\bar{\kappa}\cdot\hat{\phi}da=1$$

The time dependence $e^{j\omega t}$ is implicit.

The electromagnetic fields inside the cylinder represent solutions to Maxwell's equations subject to the boundary conditions of the problem. In differential form, Maxwell's equations are

$$\begin{aligned}\nabla\times\bar{E}&=j\omega\mu\bar{H}-\bar{\kappa}\\ \nabla\times\bar{H}&=-j\omega\varepsilon\bar{E}\end{aligned} \tag{2.2}$$

Taking the curl of the second equation and substituting in the first and the filamentary source of (2.1) results in

$$-\nabla\times\nabla\times\bar{H}\phi+\omega^2\mu\varepsilon\bar{H}\phi=-j\omega\varepsilon\delta(\rho-b)\delta(z) \tag{2.3}$$

Since the source has only a ϕ component, only the H_ϕ, E_ρ, E_z field components will be nonzero. Moreover, since the source is independent of ϕ, these field components will also be ϕ independent. This represents a field transverse magnetic with respect to the z axis. Expanding (2.3) in cylindrical coordinates results in a differential equation relating H_ϕ to the source.

$$\frac{-\partial^2 H\phi}{\partial z^2} - \frac{1}{\rho}\frac{\partial H\phi}{\partial \rho} + \left(\frac{1}{\rho^2} - k^2\right) H\phi - \frac{\partial^2 H\phi}{\partial \rho^2} = j\omega\varepsilon\delta(\rho - b)\delta(z) \tag{2.4}$$

Now define the Fourier transform of H_ϕ in the z direction as

$$h(\rho, \xi) = \int_{-\infty}^{\infty} H\phi(\rho, z) e^{-j\xi z} dz \tag{2.5a}$$

and the inverse as

$$H\phi(\rho, z) = \frac{1}{2\pi}\int_{-\infty}^{\infty} h(\rho, \xi) e^{j\xi z} dz \tag{2.5b}$$

Equation (2.4) can be reduced to a nonhomogeneous, ordinary differential equation by taking the Fourier transform of both sides in the z direction. The result is

$$-\frac{1}{\rho}\frac{\partial h}{\partial \rho} + \left(\frac{1}{\rho^2} - k^2 + \xi^2\right) h - \frac{\partial^2 h}{\partial \rho^2} = j\omega\varepsilon\delta(\rho - b) \tag{2.6}$$

Note that the z dependence has been removed and the ring has been converted to an equivalent system of cylinders.

The problem is now one of solving (2.6) subject to the transformed boundary conditions and taking the inverse transform defined by Equation (2.5b). Equation (2.6) will be solved in the next section; however, because the inverse transform is analytically very difficult, the FFT

numerical algorithm is used to invert the solution to (2.6). This computation is discussed in Section 4. The remaining field components, E_ρ and E_z, are found using Maxwell's equations, which in cylindrical coordinates for this problem are

$$E_\rho = \frac{j}{\omega\varepsilon}\frac{\partial H_\phi}{\partial z}$$
$$E_z = \frac{-j}{\omega\varepsilon}\left(\frac{\partial H_\phi}{\partial \rho} + \frac{1}{\rho}H_\phi\right) \qquad (2.7)$$

3. SOLUTION TO THE BOUNDARY VALUE PROBLEM

The solution to Equation (2.6) subject to the transformed boundary conditions is considered here. First note that for $\rho \neq b$ Equation (2.6) reduces to

$$-\frac{1}{\rho}\frac{\partial h}{\partial \rho}+\left(\frac{1}{\rho^2}-k^2+\xi^2\right)h-\frac{\partial^2 h}{\partial \rho^2}=0 \tag{3.1}$$

since the source term is zero for $\rho \neq b$. When Equation (2.6) is integrated over the region $b-\delta\rho$ to $b+\delta\rho$, the result is

$$(\xi^2-k^2)\int h\,\partial\rho-\left.\frac{h}{\rho}-\frac{\partial h}{\partial \rho}\right|_{b-\delta\rho}^{b+\delta\rho}=j\omega\varepsilon_0 \tag{3.2}$$

In the limit as $\delta\rho \to 0$, since h is continuous, both the integral term and first term in the brackets go to zero. The result is the first boundary condition

$$\left.\frac{\partial h}{\partial \rho}\right|_{\rho=b-\delta\rho}-\left.\frac{\partial h}{\partial \rho}\right|_{\rho=b+\delta\rho}=j\omega\varepsilon_0 \tag{3.3}$$

Two more boundary condtions are found by noting that H_ϕ is continuous at $\rho=a$ and at $\rho=b$; $h(\rho,\xi)$ must also be continuous at these points.

$$h(a+\delta\rho,\xi)=h(a-\delta\rho,\xi) \tag{3.4}$$

$$h(b+\delta\rho,\xi)=h(b-\delta\rho,\xi) \tag{3.5}$$

The fourth and final boundary condition is found by forcing E_z to be continuous at $\rho=a$. Using Equation (2.7) to represent $E\rho$ and equating for ρ just inside and just outside the cylinder yield

$$\left.\left(\frac{\partial H\phi}{\partial \rho}+\frac{1}{\rho}H\phi\right)\right|_{\rho=a-\delta\rho}=\varepsilon_r\left.\left(\frac{\partial H\phi}{\partial \rho}+\frac{1}{\rho}H\phi\right)\right|_{\rho=a+\delta\rho}$$

When the Fourier transform of both sides is taken according to (2.5a), the result is

$$\left.\frac{\partial h}{\partial \rho}\right|_{\rho=a-\delta\rho} -\varepsilon_r \left.\frac{\partial h}{\partial \rho}\right|_{\rho=a+\delta\rho} +(1-\varepsilon_r)\left.\frac{h}{\rho}\right|_{\rho=a} =0 \qquad (3.6)$$

where ε_r is the relative dielectric constant of the cylinder.

The next step is to write general solutions to (3.1) for each of the three regions: inside the cylinder ($0<\rho<a$), between the cylinder and the current loop ($a<\rho<b$), and outside the loop ($\rho>b$). The unknown constants, multiplying the solutions in each region, are determined by enforcing the boundary conditions (3.3) thru (3.6) and forcing the fields to be finite at $\rho=0$ and $\rho=\infty$.

The solution to Equation (3.1) has two general forms, a standing-wave solution and a traveling-wave solution given respectively by

$$h(\rho,\xi)=AJ_1(\beta\rho)+BN_1(\beta\rho) \qquad (3.7a)$$

$$h(\rho,\xi)=CH_1^{(2)}(\beta\rho)+DH_1^{(1)}(\beta\rho) \qquad (3.7b)$$

where $\beta^2=k^2-\xi^2$, $J_1(\beta\rho)$ and $N_1(\beta\rho)$ are Bessel functions of the first and second kind respectively, $H_1^{(1)}(\beta\rho)$ and $H_1^{(2)}(\beta\rho)$ are Hankel functions of the first and second kind.

First consider the region ($0<\rho<a$). Here use the standing-wave solution (3.7a). Note that in order for $h(\rho,\xi)$ to remain finite at $\rho=0$ the coefficient B must be zero since $N_1(\beta\rho)$ is infinite at $\rho=0$.

$$h(\rho,\xi)=AJ_1(\beta_1\rho) \qquad (3.8)$$

for $0<\rho<a$ and $\beta_1^2=k_1^2-\xi^2$

In the region $\rho>b$, use the travelling-wave solution and force the fields to be finite at $\rho=\infty$.

$$h(\rho,\xi)=DH_1^{(1)}(\beta_0\rho) \qquad (3.9)$$
$$\text{for } \rho>b \text{ and } \beta_0^2=k_0^2-\xi^2$$

Finally in the region $a<\rho<b$, both terms of the standing-wave solution must be used with two more unknown constants.

$$h(\rho,\xi)=CJ_1(\beta_0\rho)+EN_1(\beta_0\rho) \qquad (3.10)$$
$$\text{for } a<\rho<b \text{ and } \beta_0^2=k_0^2-\xi^2$$

The unknown constants A,C,D,E in Equations (3.8) thru (3.10) are found by applying the boundary conditions (3.3) thru (3.6). This results in four equations in four unknowns.

$$\begin{aligned}
&DH_1^{(1)}(\beta_0 b)-CJ_1(\beta_0 b)-EN_1(\beta_0 b)=0\\
&CJ_1(\beta_0 a)+EN_1(\beta_0 a)-AJ_1(\beta_1 a)=0\\
&A[\beta_1 aJ_0(\beta_1 a)-J_1(\beta_1 a)]+C[J_1(\beta_0 a)-\varepsilon_r\beta_0 aJ_0(\beta_0 a)]+E[N_1(\beta_0 a)\\
&\qquad -\varepsilon_r\beta_0 aN_0(\beta_0 a)]=0\\
&-D[\beta_0 bH_0^{(1)}(\beta_0 b)-H_1^{(1)}(\beta_0 b)]+C[\beta_0 bJ_0(\beta_0 b)-J_1(\beta_0 b)]+E[\beta_0 bN_0(\beta_0 b)\\
&\qquad -N_1(\beta_0 b)]=j\omega\varepsilon_0 b
\end{aligned} \qquad (3.11)$$

Since only the field distribution inside the cylinder is desired for this problem, only the unknown coefficient A of Equation (3.8) must be found. Some of the details of this lengthy calculation can be found in Appendix A. The result after substituting A into (3.8) is

$$h(\rho,\xi)=\frac{j\omega\varepsilon_0 bH_1^{(1)}(\beta_0 b)J_1(\beta_1\rho)}{\beta_1 aJ_0(\beta_1 a)H_1^{(1)}(\beta_0 a)-\beta_0 aJ_1(\beta_1 a)H_0^{(1)}(\beta_0 a)} \qquad (3.12)$$

Finally, $H_\phi(\rho,z)$ is found by taking the inverse Fourier transform of (3.12). The result is

$$H\phi(\rho,z)= \frac{j\omega\varepsilon_0 b}{2\pi a}\int_{-\infty}^{\infty} \frac{H_1^{(1)}(\beta_0 b)J_1(\beta_1\rho)e^{j\xi z}\partial z}{\beta_1 J_0(\beta_1 a)H_1^{(1)}(\beta_0 a)-\beta_0 J_1(\beta_1 a)H_0^{(1)}(\beta_0 a)} \qquad (3.13)$$

for $0<\rho<a$

with $\beta_0^2=k_0^2-\xi^2$

$\beta_1^2=k_1^2-\xi^2$

The numerical solution of Equation (3.13) is the subject of the next section.

4. NUMERICAL SOLUTION

The solution of (3.13) for the field component H_ϕ and the field components E_ρ and E_z is the subject of this section. The FORTRAN IV listing of the computer program written to solve (3.13) is given in Appendix B. The complex function "CF" is used to compute $h(\rho,\xi)$ of Equation (3.12) at discrete values of ξ. A plot of the function $h(\rho,\xi)$ vs. ξ for a sample configuration at a certain value of ρ is given in Figure 2. Taking the inverse transform of this curve will give H_ϕ. Note that for values of ξ above approximately 0.6 the calculation of $h(\rho,\xi)$ becomes unstable. It can be shown that in the limit for large ξ $h(\rho,\xi)$ goes to zero. The unstability occurs because both the numerator and denominator of (3.12) go to zero fairly rapidly and the limit of the computer's accuracy is quickly reached. Thus, to circumvent this problem, the function $h(\rho,\xi)$ was filtered at $\xi=0.6$ so that no numerical noise for $\xi>0.6$ would affect the inverse transform.

Prior to taking the inverse Fourier transform, additional zeros were placed on the ends of the array containing values of $h(\rho,\xi)$ to increase resolution in the space domain [9]. The number of zeros added and the total FFT array size are determined by the input variables "MULT" and "M." Taking the inverse transform gives the field component H_ϕ along a line parallel to the z axis for z values between the limits set by the input variable "PU." The inverse transform was taken using the complex International Math Science Library Fast Fourier Transform routine called "FFT2C."

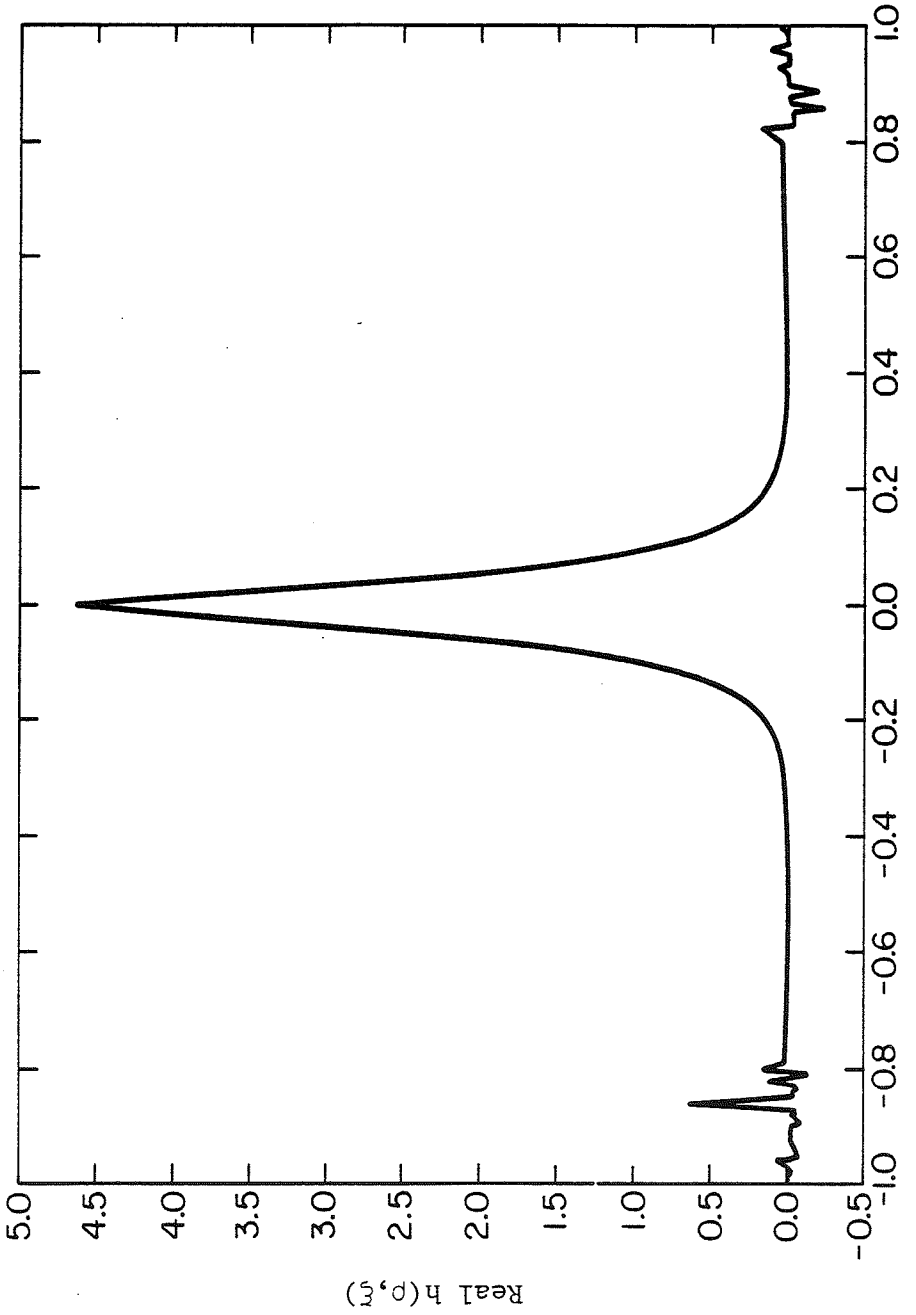

Figure 2a. Real $h(\rho,\xi)$ vs. ξ
(a=20cm, b=25cm, h_f=.03591-j.01516)

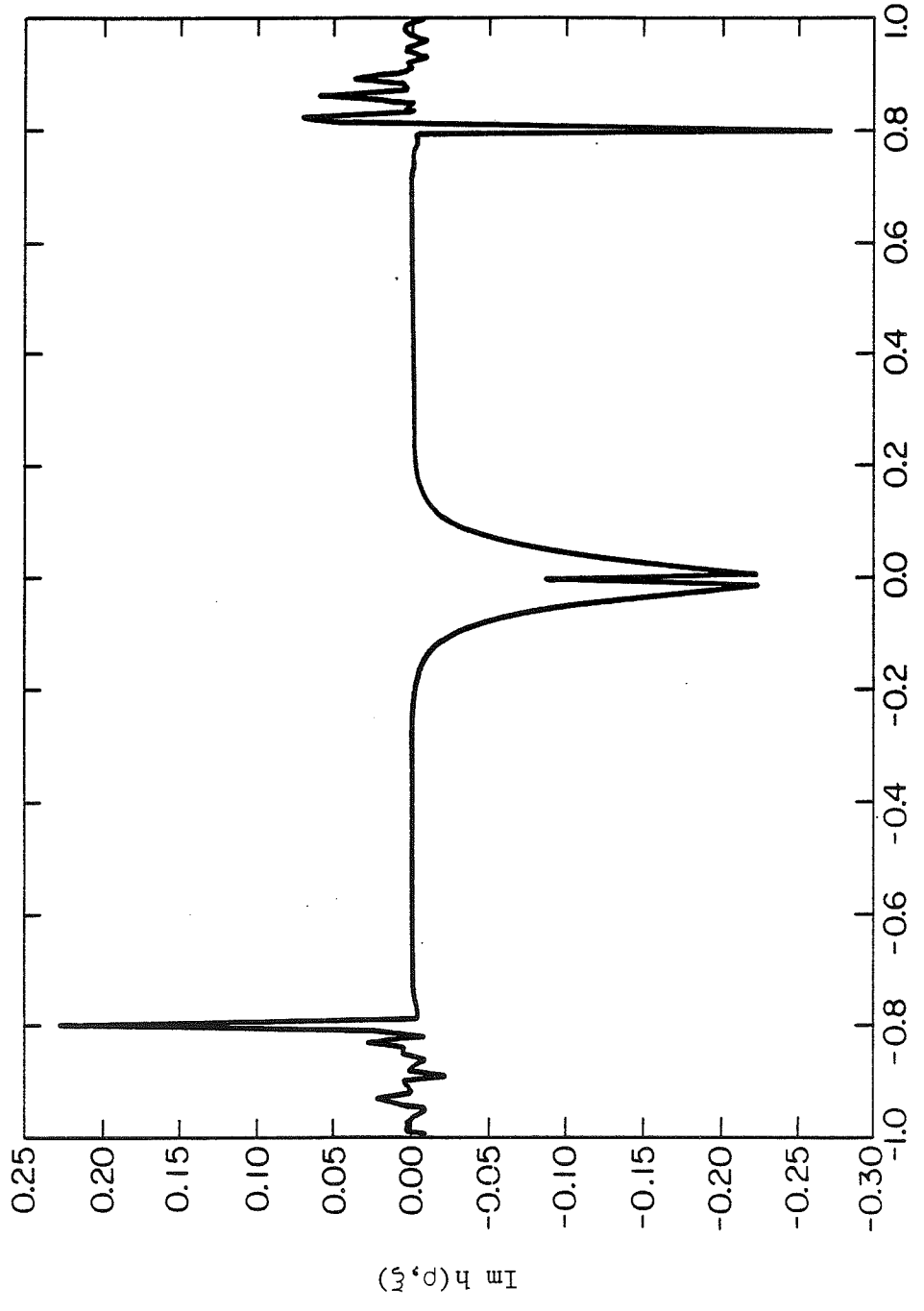

Figure 2b. Im $h(\rho,\xi)$ vs. ξ

The remaining field components E_ρ and E_z may be found by applying Equation (2.7) directly to the integrand of (3.11) and taking the inverse Fourier transform via the FFT algorithm. However, due to the highly peaked nature of these field components in the transform domain, the numerical inverse transform is difficult. It turns out that applying finite difference techniques to the inverse transform of $h(\rho,\xi)$ yields more accurate and computationally efficient results. The four-point difference technique described in [8] was used to approximate the derivative of H_ϕ with respect to ρ for E_z and z for E_ρ. The four point approximation is given by

$$\frac{\partial f(x_1)}{\partial x} \doteq \frac{1}{6h}\left\{-2f(x_0)-3f(x_1)+6f(x_2)-f(x_3)\right\} \qquad (4.1)$$

Several values of $\Delta\rho$ and Δz were used in (4.1) to calculate E_ρ and E_z. It was found that these field components were remarkably insensitive to these parameters. The results were plotted on Tektronix plotters using GCS/Future plotting software.

5. NUMERICAL RESULTS

Numerical results using the computer program listed in Appendix B are given in this section. Two different dielectric cylinders are studied at 40.68 MHz. The first has a wavenumber corresponding to fat which has a relatively low water content and thus a low loss tangent ($\varepsilon'=14.6$, $\varepsilon''=15.0$), and a second with a wavenumber corresponding to muscle tissue that has a much higher water content and a loss tangent approximately 20 times that of fat ($\varepsilon'=97.3$, $\varepsilon''=306.36$) [2]. The lossless case of a simple magnetic current ring in free space is also given for reference. Results for the lossless case were obtained by using a cylinder with the free-space wavenumber. Plots of each field component versus ρ, the radial distance, at z=0 and at z=5 centimeters for each of the three cases are given in Figures 3 thru 11 (pages 18 thru 26). The field components H_ρ and E_z are symmetric about z=0, while E_ρ exhibits a 180 degree phase reversal. A search of the published literature has yielded no similar studies for comparison with these results.

The power dissipated in a lossy dielectric that produces tissue heating in hyperthermia is a function of the total electric field squared and the conductivity of the medium [1]. The power dissipated is given by

$$P=\tfrac{1}{2}\sigma \mid E_{TOTAL} \mid^2 \ W/cm^3 \tag{5.1}$$

where σ is the conductivity. Plots of the power dissipated inside the two uniform cylinders studied here with the appropriate σ taken from [2] are given in Figures 12 and 13 (pages 27 and 28). Note that the maximum

heating occurs at the surface and is fairly constant in the central region of the cylinder. If one compares the figures for z=0 and z=5, it is found that above and below the helix the fields taper off quickly so some focusing is achieved. This is a desirable heating pattern for regional hyperthermia though surface cooling may be required.

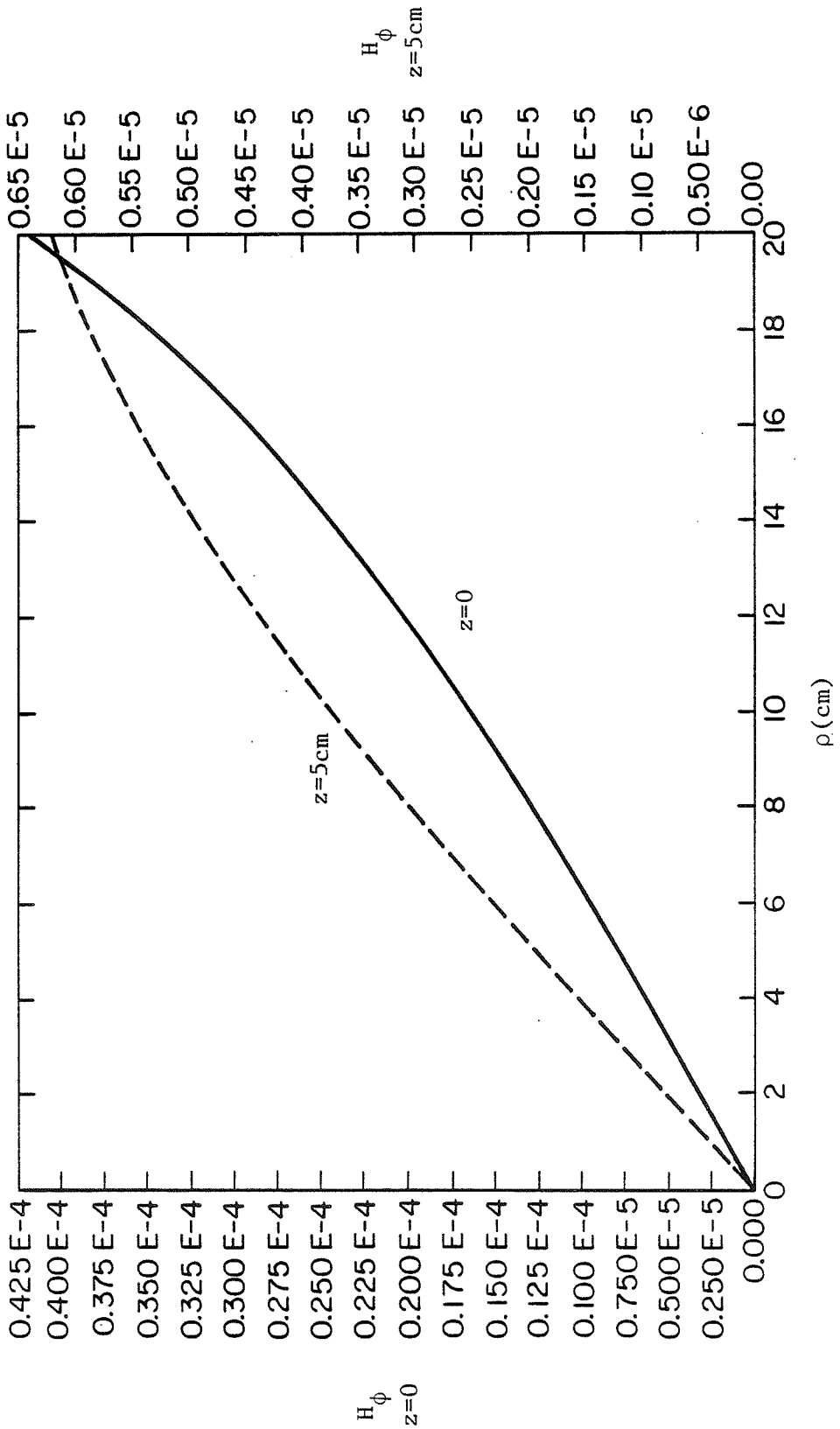

Figure 3. H_ϕ (A/cm) vs. ρ for fat tissue
(a=20cm, b=25cm, k_f=.03591-j.01516)

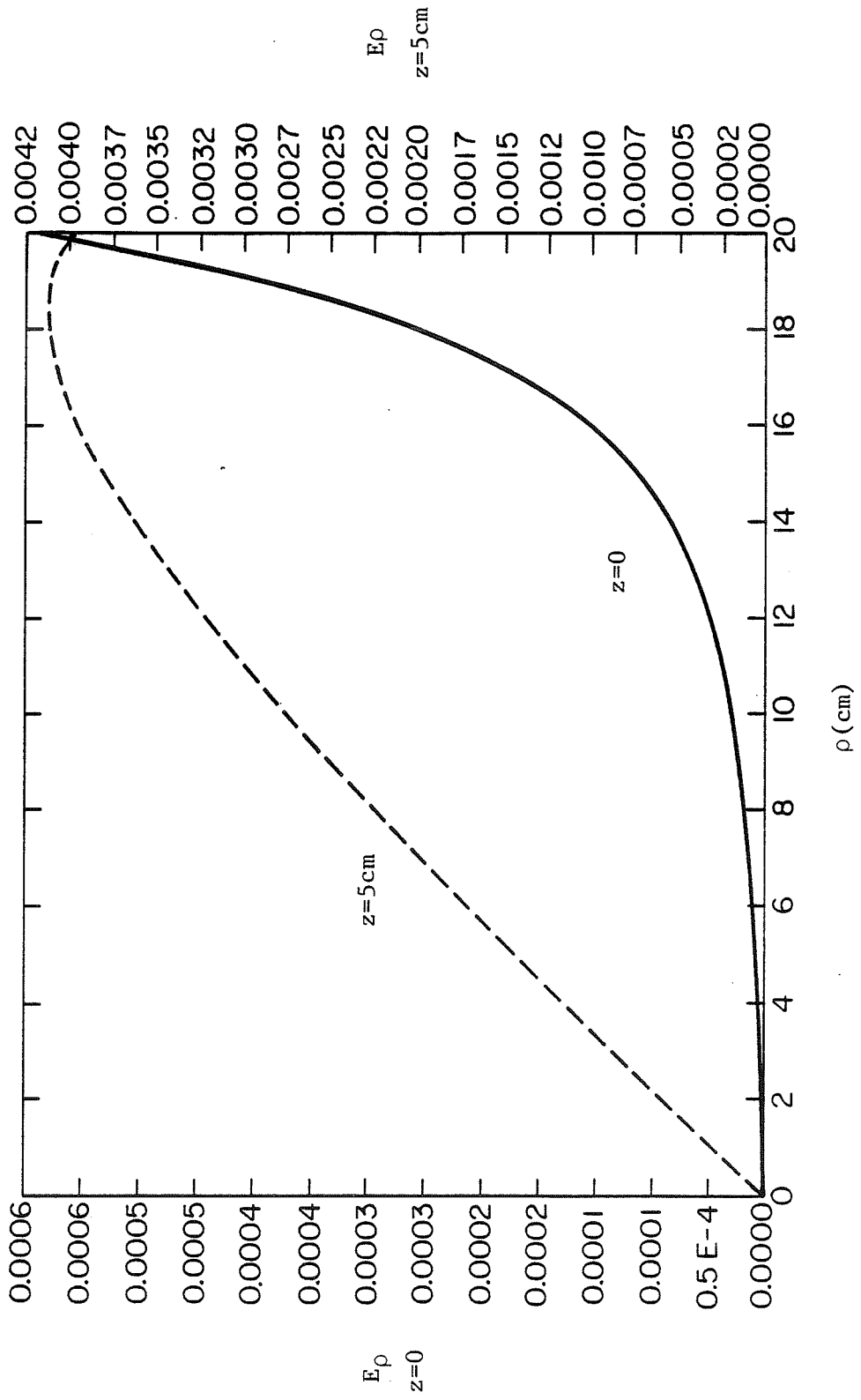

Figure 4. E_ρ (V/cm) vs. ρ
(a=20cm, b=25cm, k_f=.03591-j.01516)

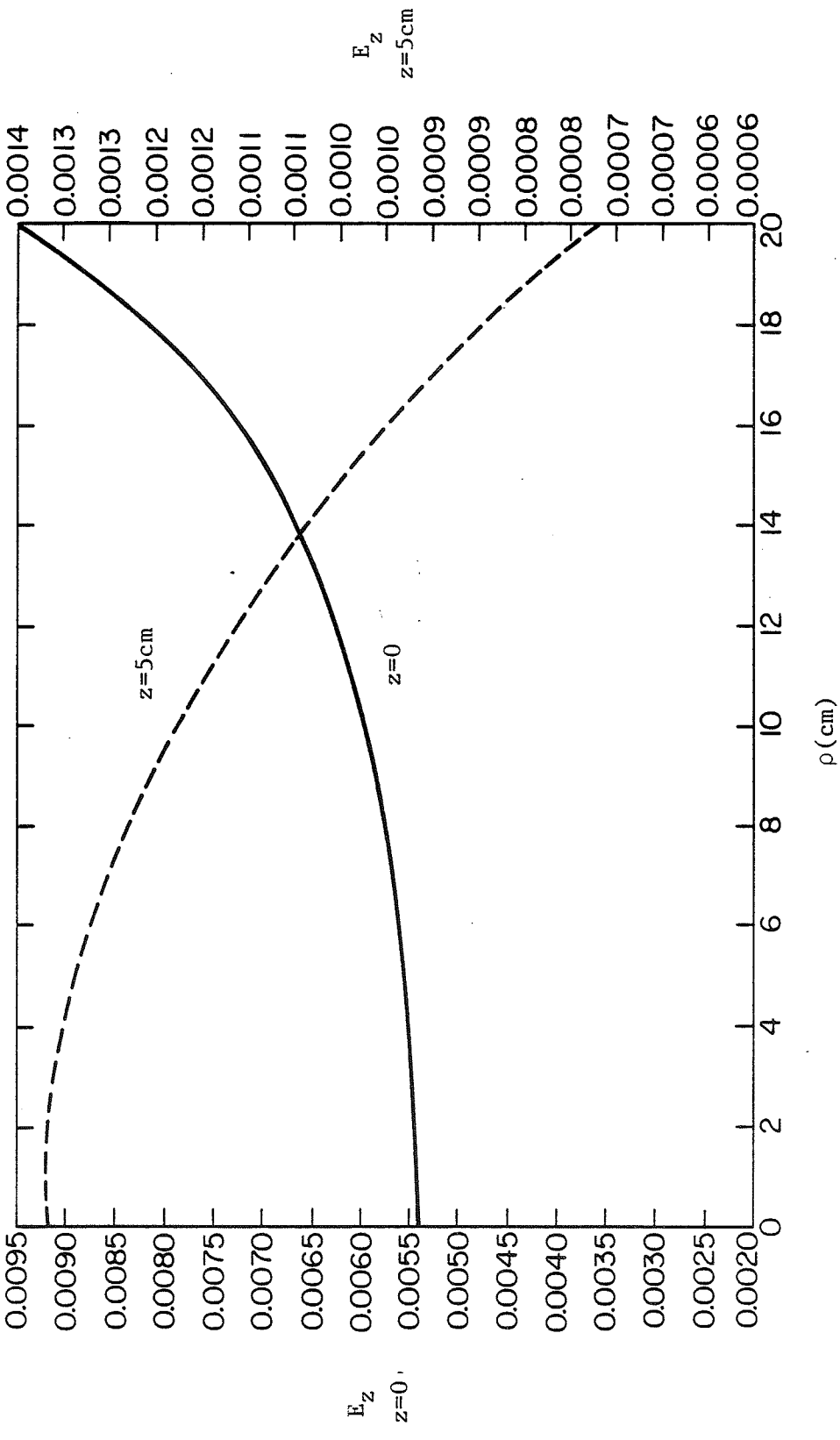

Figure 5. E_z (V/cm) vs. ρ
(a=20cm, b=25cm, k_f=.03591-j.01516)

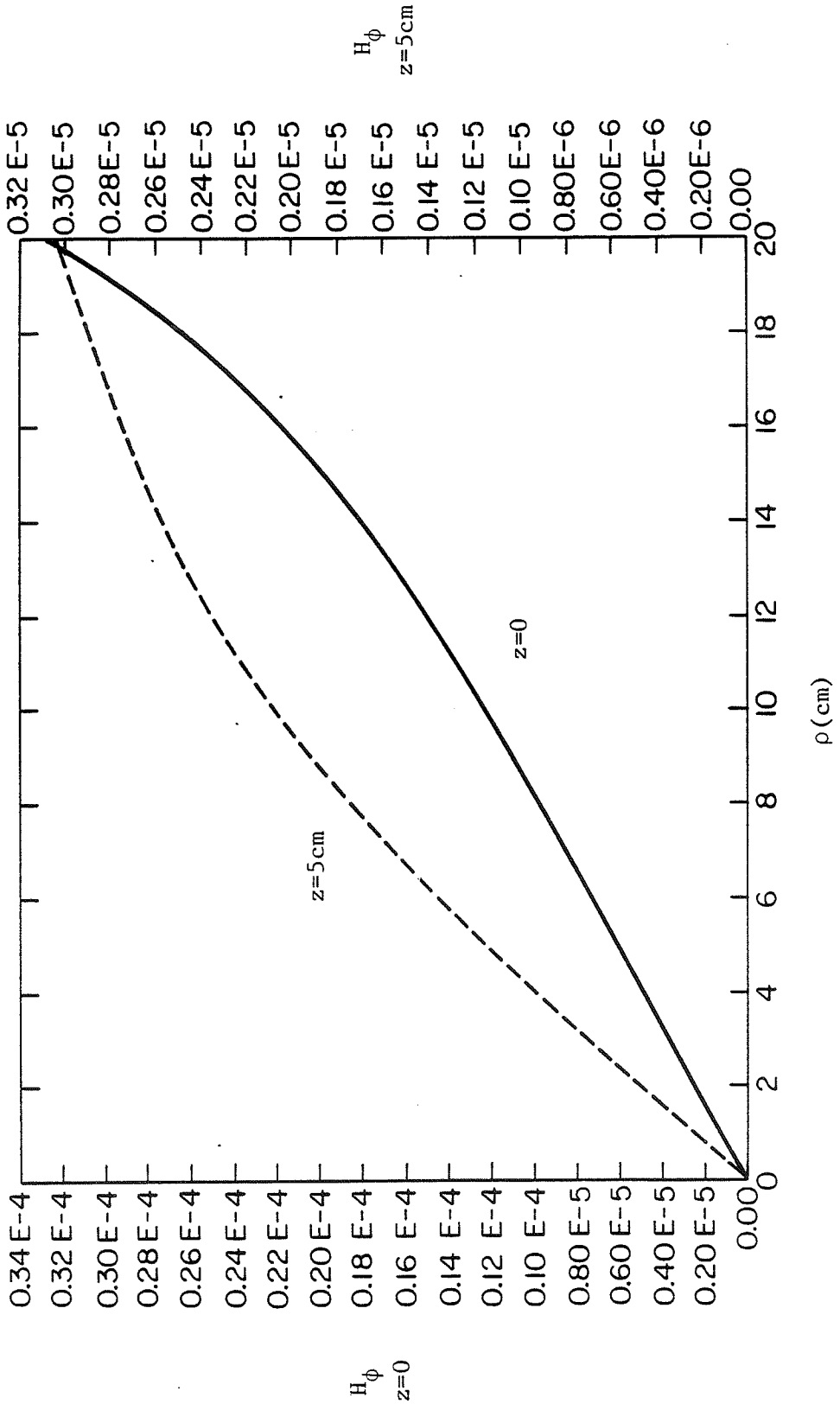

Figure 6. H_ϕ (A/cm) vs. ρ for muscle tissue
(a=20cm, b=25cm, k_m=.1232-j.09017)

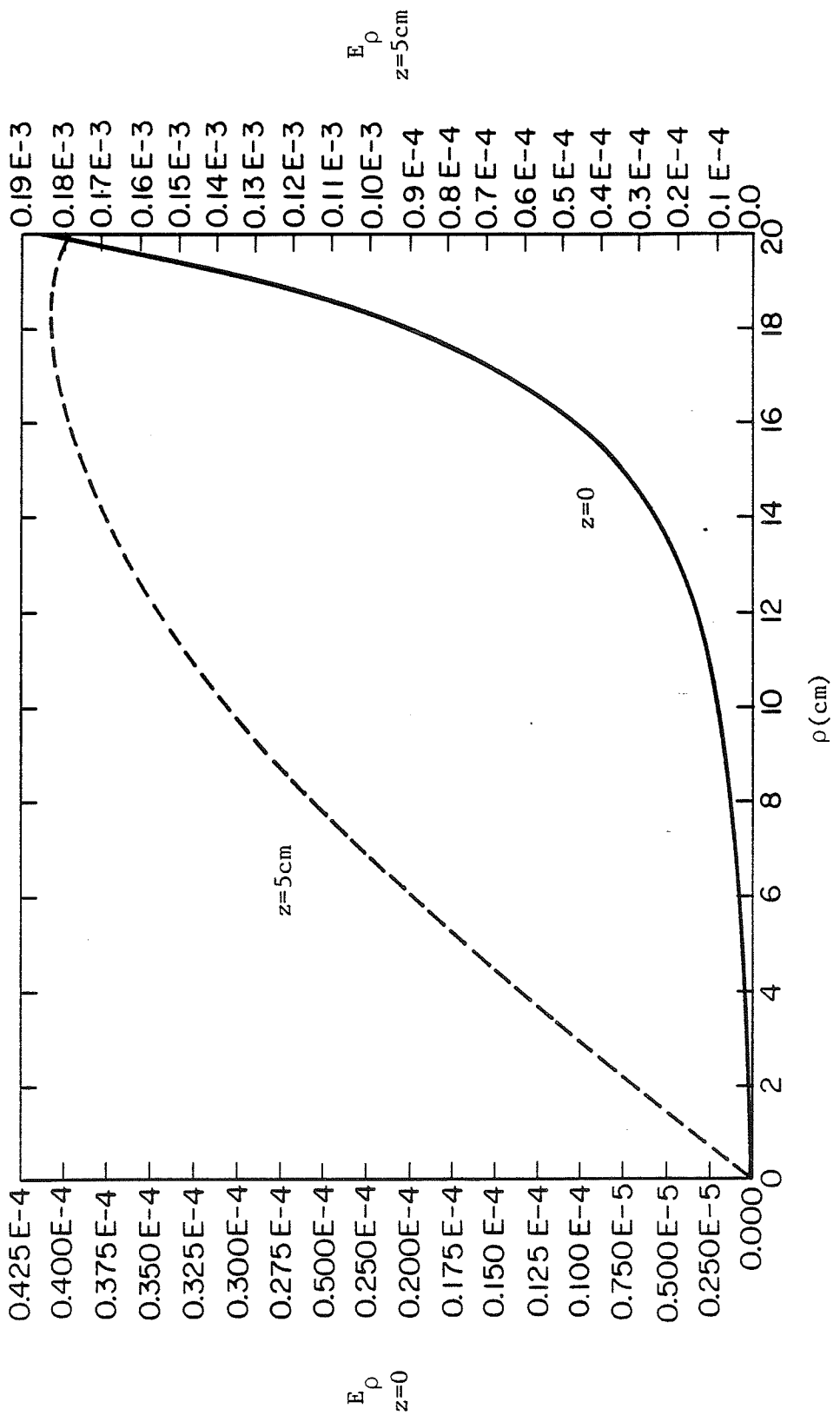

Figure 7. E_ρ (V/cm) vs. ρ
(a=20cm, b=25cm, k_m=.1232-j.09017)

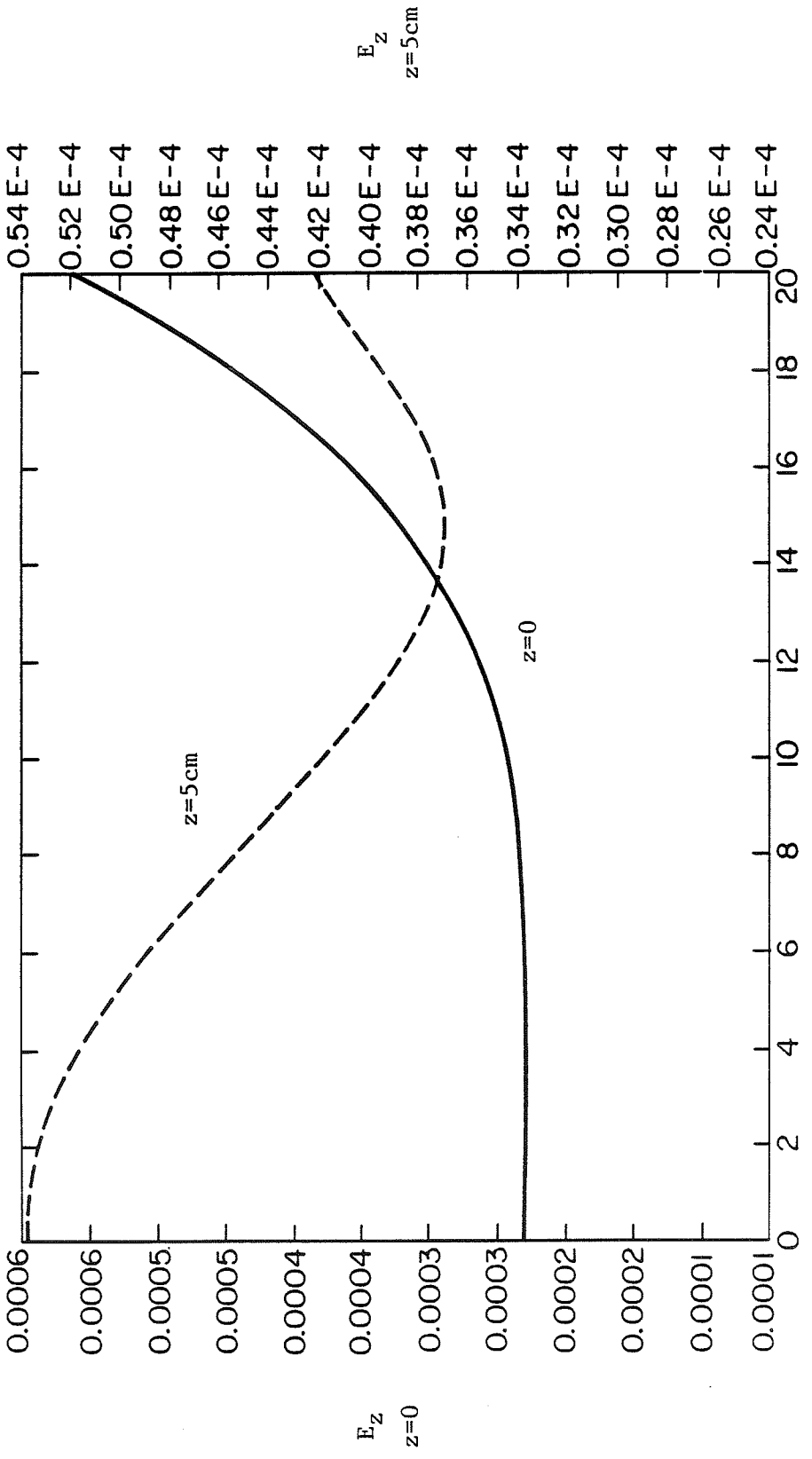

Figure 8. E_z (V/cm) vs. ρ
(a=20cm, b=25cm, k_m=.1232-j.09017)

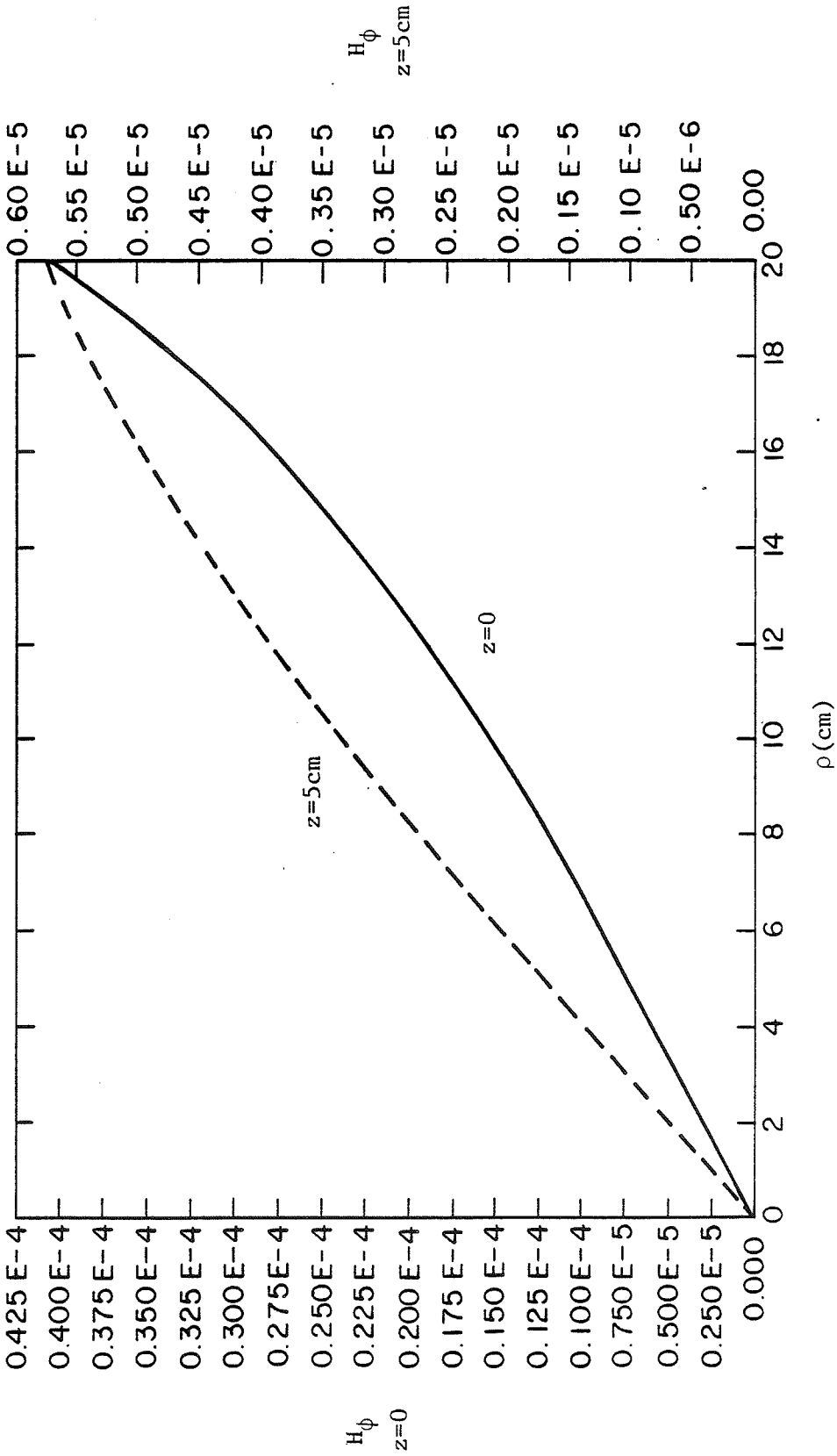

Figure 9. H_ϕ (A/cm) vs. ρ in free space
(a=20 cm, b=25cm, k_0=.00852)

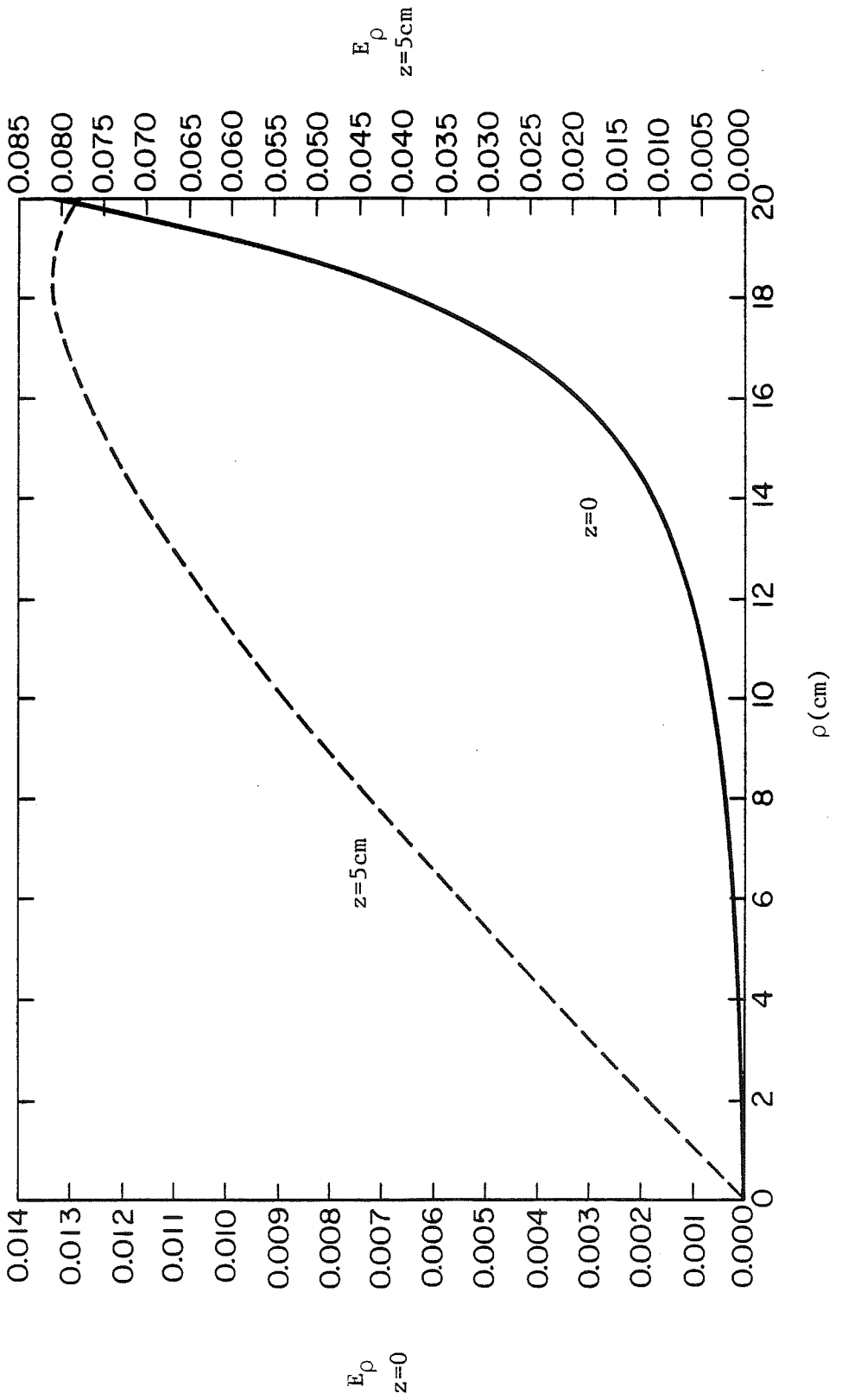

Figure 10. E_ρ (V/cm) vs. ρ
(a=20cm, b=25cm, k_0=.00852)

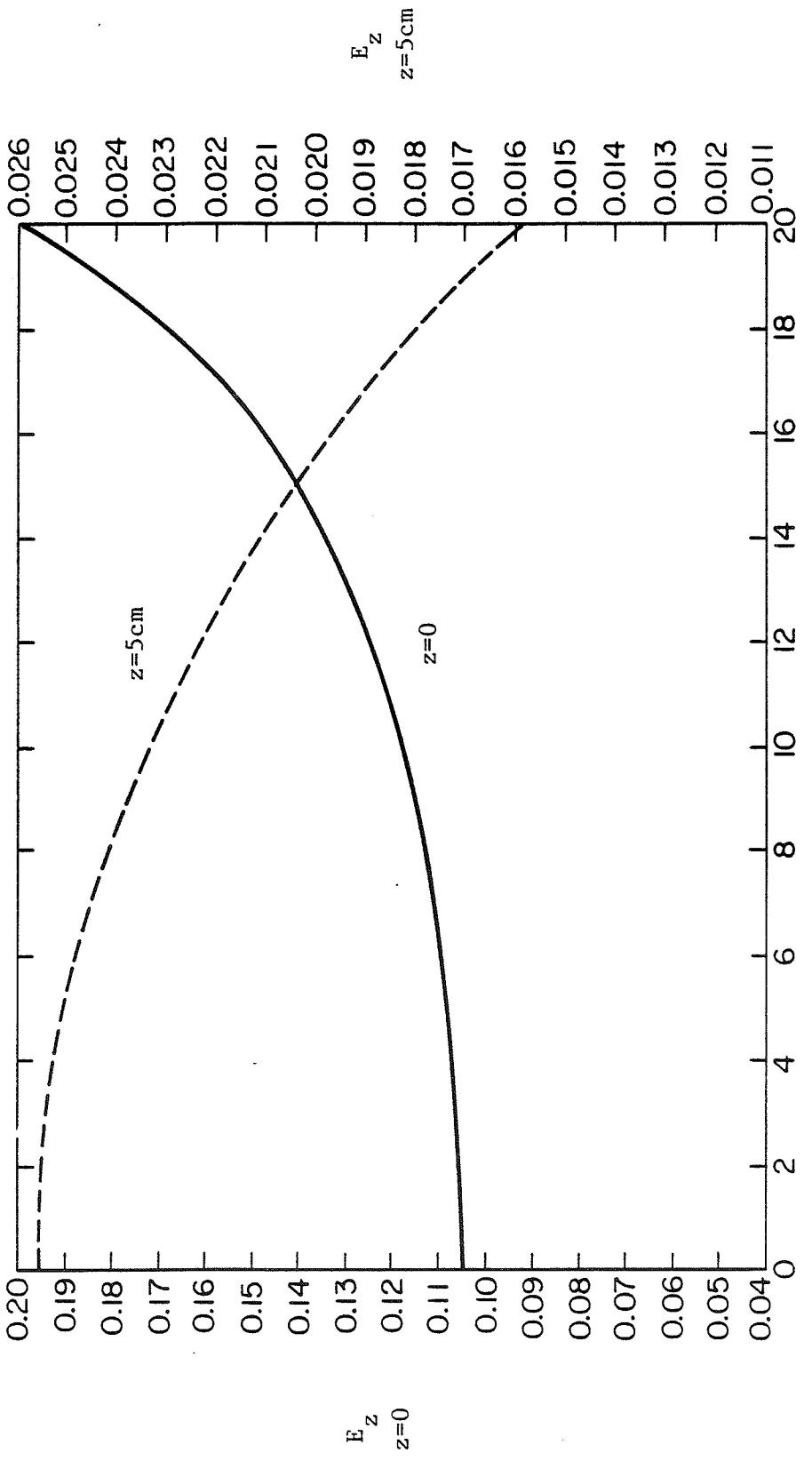

Figure 11. E_z (V/cm) vs. ρ
(a=20cm, b=25cm, k_0=.00852)

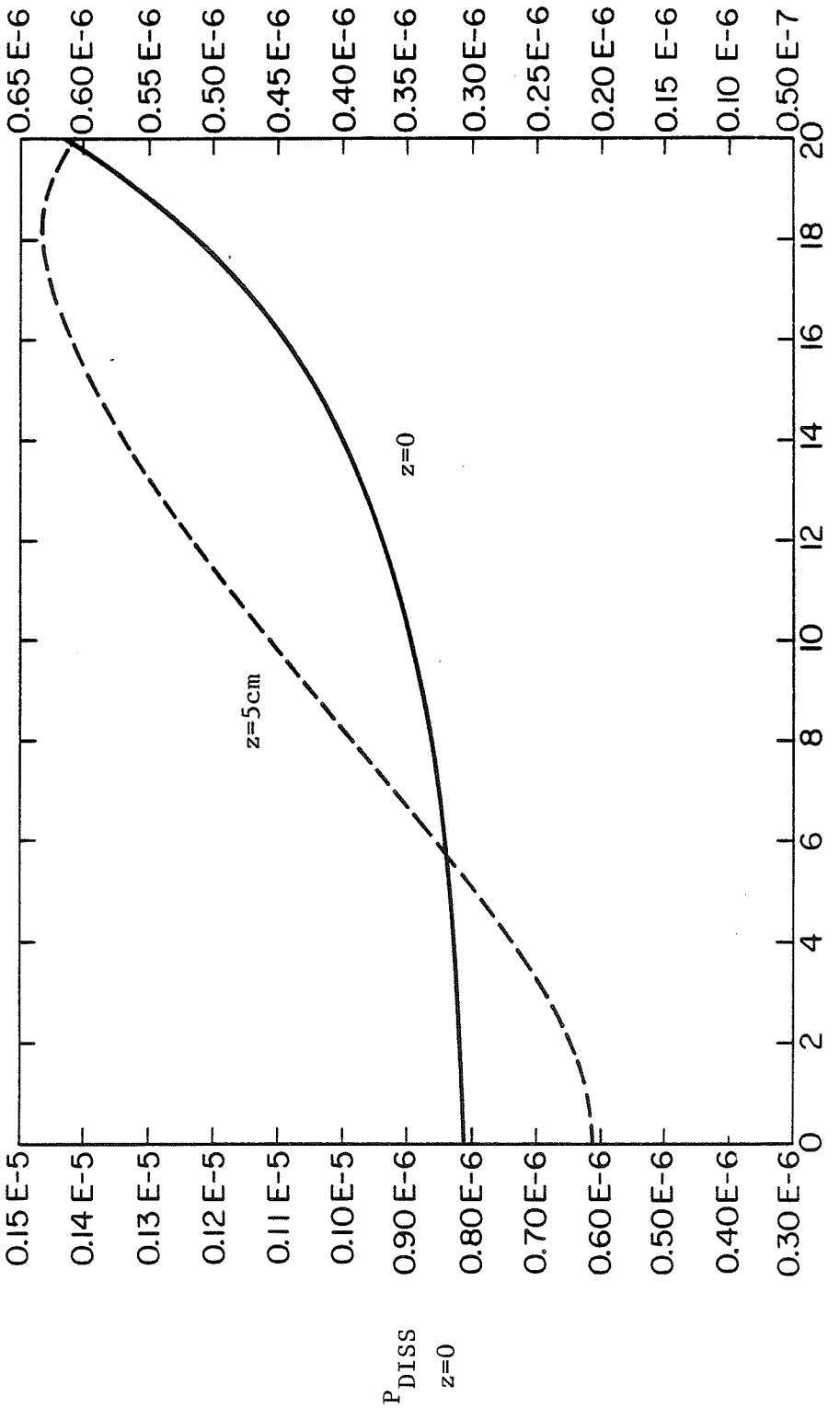

Figure 12. Power dissipated (W/cm^3) vs. ρ for fat tissue
(a=20cm, b=25cm, k_f=.03591-j.01516, σ=.0003s/m)

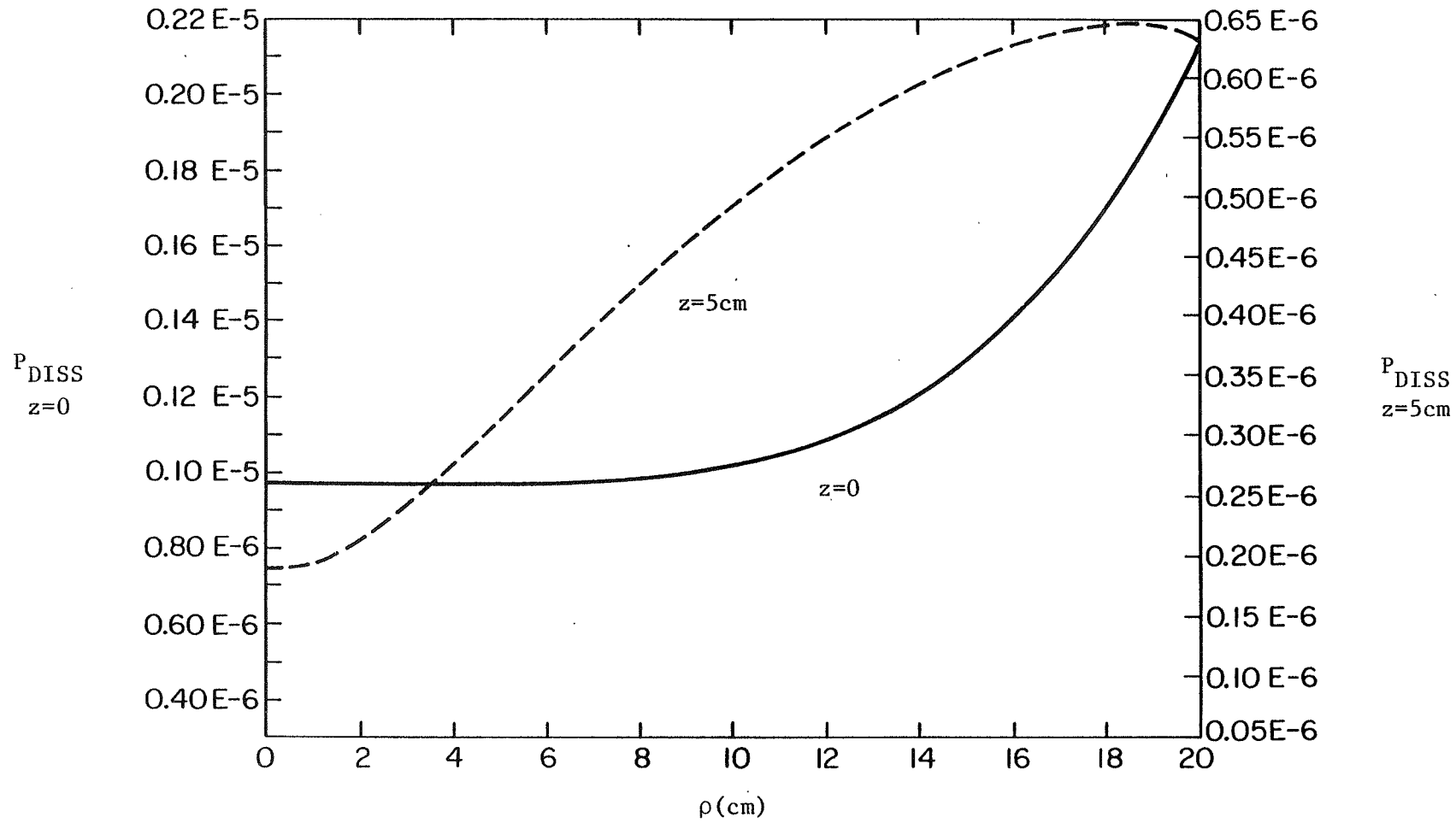

Figure 13. Power dissipated (W/cm^3) vs. ρ for muscle tissue
(a=20cm, b=25cm, k_m=.1232-j.09017, σ=.09017s/m)

6. CONCLUSION

The results of a theoretical and numerical study of the fields inside a homogeneous, lossy cylinder due to a circular helix are presented. The circular helix in this configuration is a promising applicator for short wave hyperthermia due to its reasonably good heating pattern and simple design. The helix was modeled as a filament of magnetic current, and an exact integral solution for the problem of a filamentary current around an infinite cylinder was formulated. The integral solution was inverted numerically, and the internal field distributions for the cases of a cylinder with a wavenumber corresponding to fat, muscle and free space, i.e., the problem of a ring in homogeneous free space, were presented. While surface heating was high, plots of the power dissipated, which is determined by the electric field, show that a relatively uniform heating pattern deep inside the cylinder is attainable with this type of RF applicator. Other configurations for use in this frequency range, currently in clinical tests, exhibit less desirable electric field distributions.

Further theoretical studies include the determination of the optimum frequency and dimensions of the helix and the problem of multilayered cylinders to more accurately predict the heating patterns within the human body. Experimental work should also be done to verify the results of this study.

APPENDIX A - SOLUTION FOR THE CONSTANT A OF EQUATION 3.8

In order to solve for the constant A of Equation (3.8) write Equation (3.9) in matrix form.

$$\begin{bmatrix} 0 & \Delta_{12} & \Delta_{13} & \Delta_{14} \\ \Delta_{21} & 0 & \Delta_{23} & \Delta_{24} \\ \Delta_{31} & 0 & \Delta_{33} & \Delta_{34} \\ \Delta_{42} & 0 & \Delta_{43} & \Delta_{44} \end{bmatrix} \begin{bmatrix} A \\ D \\ C \\ E \end{bmatrix} = \begin{bmatrix} 0 \\ 0 \\ 0 \\ j\omega\varepsilon_0 b \end{bmatrix} \tag{A.1}$$

where

$\Delta_{12} = H_1^{1}(\beta_0 b)$ $\quad \Delta_{13} = -J_1(\beta_0 b)$ $\quad \Delta_{14} = -N_1(\beta_0 b)$

$\Delta_{21} = -J_1(\beta_1 a)$ $\quad \Delta_{23} = J_1(\beta_0 a)$ $\quad \Delta_{24} = N_1(\beta_0 a)$

$\Delta_{31} = \beta_1 a J_0(\beta_1 a) - J_1(\beta_1 a)$ $\quad \Delta_{33} = J_1(\beta_0 a) - \varepsilon_r \beta_0 a J_0(\beta_0 a)$

$\Delta_{34} = N_1(\beta_0 a) - \varepsilon_r \beta_0 a N_0(\beta_0 a)$ $\quad \Delta_{42} = H_1^{1}(\beta_0 b) - \beta_0 b H_0^{1}(\beta_0 b)$

$\Delta_{43} = \beta_0 b J_0(\beta_0 b) - J_1(\beta_0 b)$ $\quad \Delta_{44} = \beta_0 b N_0(\beta_0 b) - N_1(\beta_0 b)$

Using Cramer's rule to solve for A

$$A = \frac{\det \bar{\bar{B}}}{\det \bar{\bar{A}}} \tag{A.2}$$

where $\bar{\bar{A}}$ is the coefficient matrix of Equation (A.1) and $\bar{\bar{B}}$ is the matrix formed by replacing the first column of $\bar{\bar{A}}$ by the right-hand side of (A.1). Solving (A.2)

$$\det \bar{\bar{B}} = -j\omega\varepsilon_0 b\{\Delta_{12}\Delta_{23}\Delta_{34} - \Delta_{33}\Delta_{24}\Delta_{12}\}$$

multiplying this out, canceling similar terms and using the Wronskian of $J_0(\beta_0 a)$ and $N_0(\beta_0 a)$ result in

$$\det \bar{\bar{B}} = \frac{j2\omega}{\pi}\varepsilon_0\varepsilon_r b H_1^{1}(\beta_0 b) \tag{A.3}$$

The denominator of (A.2) is a longer yet no more difficult calculation. The procedure is as follows

$$\det \bar{\bar{A}} = -\Delta_{21}\Delta_{12}\Delta_{33}\Delta_{44} - \Delta_{13}\Delta_{34}\Delta_{42}\Delta_{21}$$
$$+ \Delta_{21}\Delta_{42}\Delta_{33}\Delta_{14} + \Delta_{21}\Delta_{43}\Delta_{34}\Delta_{12}$$
$$+ \Delta_{31}\Delta_{12}\Delta_{23}\Delta_{44} + \Delta_{31}\Delta_{13}\Delta_{24}\Delta_{42}$$
$$- \Delta_{31}\Delta_{42}\Delta_{23}\Delta_{14} - \Delta_{31}\Delta_{43}\Delta_{24}\Delta_{12}$$

Multiplying this out, canceling similar terms and using the Wronskians for $H_0^{(1)}(\beta_0 b)$ and $J_0(\beta_0 b)$ and for $H_0^{(1)}(\beta_0 b)$ and $N_0(\beta_0 b)$ results in

$$\det \bar{\bar{A}} = -\frac{2\varepsilon_r \beta_0 a}{\pi} J_1(\beta_1 a) H_0^{(1)}(\beta_0 a) + \frac{2\varepsilon_r \beta_1 a}{\pi} J_0(\beta_1 a) H_1^{(1)}(\beta_0 a) \qquad \text{(A.4)}$$

Substituting (A.3) and (A.4) into (A.2)

$$A = \frac{j\omega\varepsilon_0 b H_1^{(1)}(\beta_0 b)}{\beta_1 a J_0(\beta_1 a) H_1^{(1)}(\beta_0 a) - \beta_0 a J_1(\beta_1 a) H_0^{(1)}(\beta_0 a)}$$

APPENDIX B- FORTRAN IV LISTING OF COMPUTER PROGRAM

```
      PROGRAM CYLDER2 (INPUT,OUTPUT,TAPE6=OUTPUT,TAPE5=INPUT)

C     THIS PROGRAM COMPUTES THE FIELDS INSIDE AN INFINITE
C     CYLINDER DUE TO A LOOP OF MAGNETIC CURRENT AROUND THE
C     CYLINDER

C     K1 = WAVE NUMBER FOR CYLINDER
C     K0 = FREE SPACE WAVE NUMBER
C     N = NUMBER OF POINTS IN FFT ARRAY
C     M = NUMBER OF STAGES IN FFT
C     PSI = TRANSFORM DOMAIN FREQUENCY VARIABLE
C     PU = UPPER LIMIT OF Z
C     MULT = REDUCES SAMPLING INTERVAL IN TRANSFORM DOMAIN
C          (A INTEGER NUMBER ROUGHLY BETWEEN 1 AND 6)
C     NP2 = NUMBER OF SAMPLES IN RANGE OF Z
C     RHO = RADIUS AT WHICH H SUB PHI IS CALCULATED
C     A = RADIUS OF CYLINDER
C     B = RADIUS OF MAGNETIC LOOP, NOTE B>A MUST BE TRUE
C     CONST =  J*W*B/(TWOPI*A)
C     CONST2 = J/W*E
C     ZZ = H SUB PHI IN SPACIAL DOMAIN
C     B0 = SQRT(K0**2-PSI**2)
C     B1 = SQRT(K1**2-PSI**2)
C     LIBRARIES USED ARE IMSL, AMOSLIB, GCS/FUTURE


      EXTERNAL CF
      COMPLEX K1, CF, CONST, Y(1025), ZZ(4,1027), CONST2, TEMP
      REAL K0, MULT
      DIMENSION X(1024), IWK(11)
      COMMON /CONSTS/ A, B, K0, K1
      PI=4.*ATAN(1.)
      TWOPI=2.*PI
      K0=0.00568
      NR=1

      WRITE (6,15)
15    FORMAT (/" ENTER K1")
      READ (5,*) RK1, XK1
      K1=CMPLX(RK1,XK1)
      WRITE (6,20)
20    FORMAT(/" ENTER UPPER LIMIT OF Z, MULTIPLIER, AND RHO")
      READ (5,*) PU, MULT, RHO
      WRITE(6,22)
22    FORMAT(/" ENTER RADIUS OF CYLINDER, RADIUS OF LOOP AND M")
```

```
      READ (5,*) A,B,M

      WRITE (6,23)
23    FORMAT(/" WHICH GRAPHS? H-PHI, E-Z, E-RHO; 1=YES")
      READ (5,*) IFLAG1, IFLAG2, IFLAG3
      IF (IFLAG2.NE.1) GO TO 33
      WRITE(6,32)
32    FORMAT(/" ENTER DELTA-RHO FOR THE CALCULATION OF E-Z")
      READ(5,*) DRHO
33    CONTINUE

      N=2**M
      XN=FLOAT(N)
      NH=N/2
      NH1=NH+1
      CONST=CMPLX(0.,2.26E-5*B/A)
      CONST2=CMPLX(0.,1.)/(K1*K1*0.31133)
      RHO1=RHO
      CALL USTART

      DO 100 I=1,4
         DO 25 J=1,NH1
            PSI=FLOAT(J-1)/(2.*PU*MULT*MULT)
            IF (PSI.LT.0.6) Y(J)=CONST*CF(RHO,PSI)
            IF (PSI.GE.0.6) Y(J)=CMPLX(0.,0.)
            IF (J.GT.NH) GO TO 25
            JJ=N+2-J
            Y(JJ)=Y(J)
25       CONTINUE

C        COMPUTE INVERSE FOURIER TRANSFORM OF Y ARRAY
C        FFT2C IS AN IMSL ROUTINE THAT COMPUTES DISCRETE
C        FOURIER TRANSFORMS

         CALL FFT2C(Y,M,IWK)
C
         DO 40 J=1,NH
            JJ=J+NH
            ZZ(I,J)=Y(JJ)/(2.*PU*MULT*MULT)
            ZZ(I,JJ)=Y(J)/(2.*PU*MULT*MULT)
40       CONTINUE
         ZZ(I,N+1)=ZZ(I,N)
         ZZ(I,N+2)=ZZ(I,N)
         ZZ(I,N+3)=ZZ(I,N)

C        COMPUTE, PLOT H-PHI, E-Z, OR E-R ACCORDING TO IFLAGS
C        DETERMINE NUMBER OF POINTS IN RANGE OF Z, FILL ARRAY
C        WITH Z VALUES FOR PLOTTING

         NP=IFIX(XN/(2.*MULT*MULT))
         NP2=2*NP
         DO 43 J=1,NP2
```

```
            X(J)=FLOAT(J-1-NP)*2.*PU*MULT*MULT/XN

43          CONTINUE

C           H-PHI FIRST

            IF (IFLAG1.NE.1) GO TO 50
            DO 45 J=1,NP2
               JJ=NH-NP+J
               Y(J)=ZZ(I,JJ)
45          CONTINUE
            CALL PLOTIT(X,Y,NP2,"Z;","H SUB PHI;")
            IFLAG1=0

C           E-R NEXT, USING FINITE DIFFERENCE TO APPROX DERIVATIVE
C           W.R.T. Z; MULTIPLY BY J/(W*E)

50          IF (IFLAG3.NE.1) GO TO 60
            DO 55 J=1,N
               TEMP=-2.*ZZ(I,J)-3.*ZZ(I,J+1)+6.*ZZ(I,J+2)-ZZ(I,J+3)
               Y(J+1)=TEMP*CONST2*XN/(12.*PU*MULT*MULT)
55          CONTINUE
            Y(1)=Y(2)
            DO 57 J=1,NP2
               JJ=NH-NP+J
               Y(J)=Y(JJ)
57          CONTINUE
            CALL PLOTIT(X,Y,NP2,"Z;","E SUB R;")
            IFLAG3=0

C           LOOP 4 TIMES FOR THE CALCULATION OF E-Z
C           THE DERIV WILL BE APPROXIMATED LATER

60          IF(IFLAG2.NE.1) GO TO 200
            RHO=RHO+DRHO
            IF(I.EQ.?) RHO=RHO-3.*DRHO
100      CONTINUE

C        USE FINITE DIFFERENCE TO APPROX DERIVATIVE W.R.T. RHO
C        ADD TO H-PHI/RHO AND MULTIPLY BY -J/(W*E)

         DO 105 J=1,N
            TEMP=-2.*ZZ(4,J)-3.*ZZ(1,J)+6.*ZZ(2,J)-ZZ(3,J)
            TEMP=TEMP/(6.*DRHO)
            Y(J+1)=-CONST2*(TEMP+ZZ(1,J+1)/RHO1)
105      CONTINUE
         Y(1)=Y(2)
         DO 110 J=1,NP2
            JJ=NH-NP+J
            Y(J)=Y(JJ)
110      CONTINUE
         CALL PLOTIT(X,Y,NP2,"Z;","E SUB Z;")
```

```
      CALL UEND
200   STOP
      END


C     'PLOTIT' PLOTS THE XN POINTS IN  Y ARRAY VS. X ARRAY
C     THE CONTENTS OF 'XLAB' AND 'YLAB' ARE THE LABELS ON THE
C     X AND Y AXES
C     GCSTEKT/FUTURE ROUTINES ARE USED

      SUBROUTINE PLOTIT(X,Y,N,XLAB,YLAB)
      DIMENSION X(1024), RY(1024), XY(1024)
      INTEGER XLAB,YLAB
      COMPLEX Y(1024)
      XN=FLOAT(N)
      DO 10 I=1,N
         RY(I)=CABS(Y(I))
         XY(I)=ATAN2(AIMAG(Y(I)),REAL(Y(I)))
         XY(I)=XY(I)*360./6.28
10    CONTINUE
      CALL UERASE
      CALL URESET
      CALL UDAREA(0.,7.49,0.,5.71)
      CALL USET("NOORIGIN")
      CALL USET("XBOTH")
      CALL USET("YBOTH")
      CALL UPSET("XLABEL",XLAB)
      CALL UPSET("YLABEL",YLAB)
      CALL UPLOT1(X,RY,XN)
      CALL UPAUSE
      CALL UERASE
      CALL URESET
      CALL UDAREA(0.,7.49,0.,5.71)
      CALL USET("NOORIGIN")
      CALL UPLOT1(X,XY,XN)
      CALL UPAUSE
      RETURN
      END


C     THIS FUNCTION COMPUTES H SUB PHI IN THE TRANSFORM DOMAIN.
C     TAKING THE FOURIER TRANSFORM OF THIS FUNCTION AND
C     MULTIPLING BY A FEW CONSTANTS WILL GIVE H SUB PHI
C     AMOSLIB ROUTINES ARE USED

      COMPLEX FUNCTION CF(RHO,PSI)
      COMMON /CONSTS/ A, B, K0, K1
      REAL K0
```

```
      COMPLEX Z, J, K1, B0, B1, J0B1A, J1B1A, H1B0A, H0B0A,
     >     H1B0B, J1B1R, CJ0, CJ1, CY0, CY1, CH0, CH1, T1
      J=CMPLX(0.,1.)
      T1=K1*K1-PSI*PSI
      T2=SQRT(CABS(T1))
      T3=0.5*ATAN2(AIMAG(T1),REAL(T1))
      B1=CMPLX(T2*COS(T3),T2*SIN(T3))
      T0=K0*K0-PSI*PSI
      IF(T0.LT.0.) B0=J*SQRT(-T0)
      IF(T0.GE.0.) B0=SQRT(T0)
      Z=B1*A
      CALL CJ01BS(Z,J0B1A,J1B1A)
      Z=B0*A
      CALL CJYHBS(Z,1,CJ0,CJ1,CY0,CY1,CH0,CH1)
      H0B0A=CJ0+J*CY0
      H1B0A=CJ1+J*CY1
      Z=B0*B
      CALL CJYHBS(Z,1,CJ0,CJ1,CY0,CY1,CH0,CH1)
      H1B0B=CJ1+J*CY1
      Z=B1*RHO
      CALL CJ01BS(Z,CJ0,J1B1R)
      CF=H1B0B*J1B1R/(B1*J0B1A*H1B0A-B0*J1B1A*H0B0A)
      RETURN
      END
```

REFERENCES

[1] D.A. Christensen and C.H. Durney, "Hyperthermia Production for Cancer Therapy: A Review of Fundamentals and Methods," Journal of Microwave Power, vol. 16, no. 2, pp. 89-105, June 1981.

[2] C.C. Johnson and A.W. Guy, "Nonionizing Electromagnetic Wave Effects in Biological Materials and Systems," Proc. IEEE, vol. 60, no. 6, pp. 692-717, June 1972.

[3] Te-Kao Wu and L.L. Tsai, "Electromagnetic Fields Induced Inside Arbitrary Cylinders of Biological Tissue," IEEE Trans. Microwave Theory Tech., vol. MTT-25, no. 1, pp. 61-65, January 1972.

[4] N. Morita and J.B. Andersen, "Near Field Absorption in Circular Cylinders from Electric and Magnetic Line Sources," Bioelectromagnetics, vol. 3, no. 2, pp. 253-274, 1982.

[5] E.C. Jordan and K.G. Balmain, Electromagnetic Wave and Radiating Systems. Englewood Cliffs, New Jersey: Prentice-Hall, 1968, p. 303.

[6] J.W. Duncan, "The Efficiency of Excitation of a Surface Wave on a Dielectric Cylinder," IEEE Trans. Microwave Theory Tech., vol. MTT-7, no. 2, pp. 257-268, April 1959.

[7] E. Jahnke and F. Emde, Tables of Functions. New York: Dover Publications, 1945, p. 146.

[8] M. Abramowitz and I.A. Stegun, Eds., Handbook of Mathematical Functions (Applied Mathematics Series 55). Washington, D.C.: NBS, 1972, p. 914.

[9] A.V. Oppenheim and R.W. Schafer, Digital Signal Processing. Englewood Cliffs, New Jersey: Prentice-Hall, 1975.